Predictive Control Method With Future Zero-Sequence Voltage to Reduce Switching Losses in Three-Phase Voltage Source Inverters

Sangshin Kwak, *Member, IEEE*, and Jun-Cheol Park

***Abstract*—This paper proposes a predictive control method with zero-sequence voltage injection to efficiently reduce the switching losses of three-phase voltage source inverters (VSIs). In the proposed predictive control method, three-phase future voltage references modified by a zero-sequence voltage injection are generated to clamp one of the three legs with the largest load current. Furthermore, the future zero-sequence voltage, which is produced online with the future voltage and current references in every sampling period, optimally adjusts the clamping duration on each leg, depending on the load angle. In addition, the proposed method selects the zero vector on the basis of the polarity of the future zero-sequence voltage to reduce the switching losses. Using a predefined cost function, the proposed predictive control scheme chooses one optimal voltage state closest to the future voltage references modified by the zero-sequence voltage injection. Therefore, the proposed predictive control method can perform load current control and minimize the switching losses of the VSI under any load condition regardless of the load angle.**

***Index Terms*—Predictive control, switching losses, voltage source inverter (VSI), zero-sequence voltage.**

I. Introduction

THREE-PHASE current-controlled voltage source inverters (VSIs), shown in Fig. 1, have been considered as the most popular structure for supplying three-phase loads. Accordingly, the proportional–integral (PI) control methods with distinct pulse-width modulation (PWM) blocks and the nonlinear hysteresis current controls have been widely employed in current-controlled VSIs [1], [2]. Recently, the predictive control method based on the finite-control-set concept has been developed as a simple and effective current control technique for VSIs owing to its simplicity without using any individual PWM blocks as well as its control flexibility [3]–[13]. By using the fundamental principle that a VSI can only apply seven different voltage states to the loads, the predictive control method predicts the seven possible future load current behavior patterns of the VSI on the basis of the load dynamic model of the VSI.

Manuscript received December 13, 2013; revised January 23, 2014; accepted January 29, 2014. Date of publication February 5, 2014; date of current version October 15, 2014. This work was supported in part by the Basic Science Research Program through the National Research Foundation of Korea funded by the Ministry of Education, Science, and Technology (2011-0013884) and (2009-0068746). Recommended for publication by Associate Editor F. W. Fuchs.

The authors are with the Department of Electrical and Electronics Engineering, Chung-Ang University, Seoul 156-756, Korea (e-mail: sskwak@cau.ac.kr).

Color versions of one or more of the figures in this paper are available online at http://ieeexplore.ieee.org.

Digital Object Identifier 10.1109/TPEL.2014.2304719

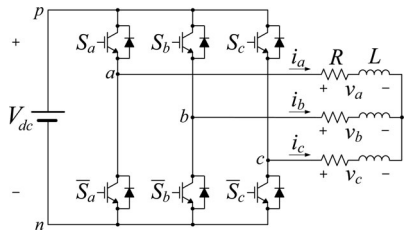

Fig. 1. VSI structure.

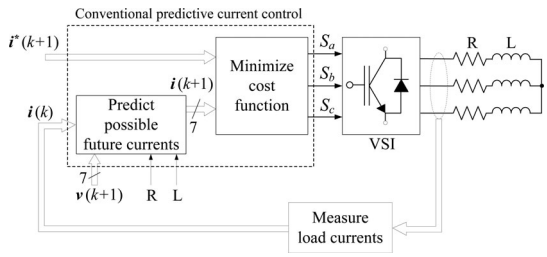

Fig. 2. Concept of the conventional predictive control method of the VSI.

Among the seven possible states, the controller evaluates all the predicted current values using a predefined cost function to select an optimal switching state to minimize the error between the future load current and the reference, as shown in Fig. 2.

On the other hand, high efficiency with reduced switching losses is as primarily important as the current-tracking capability of the VSIs. One solution to reduce the switching losses in the VSIs is adding zero-sequence voltages to the three-phase voltage references, which results in discontinuous PWMs (DPWMs) [14], [15]. Theoretically, by clamping one phase of the three VSI legs with a suitable zero-sequence voltage injection, the DPWMs can yield an average 33% reduction in the switching losses compared with the continuous PWM [14]. Several DPWM methods have been presented to reduce the switching losses of the VSIs, which reduce the switching losses with loads operating at different load angles [14], [15]. However, the current-controlled VSI with a predictive control method as shown in Fig. 2 is based on the load currents and the references. As a result, reducing the switching losses by clamping one of the three VSI legs with a proper zero-sequence voltage injection is not straightforward in the current-controller VSI with the predictive control method, in contrast to the conventional PI current controllers.

This paper proposes a predictive control method with future zero-sequence voltage injection to effectively reduce the

switching losses of the VSIs. The proposed scheme generates three-phase modified future voltage references, which adds the common future zero-sequence voltage to the three-phase future voltage references produced by an inverse dynamic model. The three-phase future voltage references modified by the zero-sequence voltage injection clamp one of the three VSI legs with the largest load current to either the positive or negative dc-bus bar. Furthermore, the future zero-sequence voltage, which is produced online with the future voltage and current references, automatically determines the clamping leg and the clamping region on the basis of the sampling period. By injecting the online future zero-sequence voltage, the clamping regions with no switching operation adaptively move or split, depending on the load angle, to prevent the leg with the largest load current from being switched at any instant. In addition, the proposed predictive control method determines how to optimally select a zero vector between the two zero vectors in terms of the switching losses using the future zero-sequence voltage. By selecting one optimal voltage state closest to the future voltage references modified by the zero-sequence voltage injection using a cost function, the proposed predictive control method can perform load current control and minimize the switching losses of the VSIs. Practical consideration to compensate for the unavoidable calculation delay present in the digital signal processor (DSP) is also presented based on the inverse dynamic model. The simulation and experimental results with a three-phase VSI are presented to validate the proposed predictive control method.

II. Proposed Predictive Control Method With Zero-Sequence Voltage Injection to Reduce Switching Losses

A. Description of the VSI Model

In the three-phase VSI shown in Fig. 1, eight voltage vectors, including six active and two zero vectors, are generated by eight switching combinations to adjust the load currents [3], [4]. The switching functions of the switches take on binary values "1" and "0" in the closed and open states, respectively. The lower switches have the complementary values of their upper switches. Because of the redundancy of the two zero vectors that generate equal output voltage vector, only seven control elements are available in the finite control set of the three-phase VSI.

The load current dynamic of the three-phase VSI with a general three-phase resistive–inductive load is expressed in a vector form in the *abc* frame as

$$\boldsymbol{v}_{abc} = R\boldsymbol{i}_{abc} + L\frac{d\boldsymbol{i}_{abc}}{dt} \tag{1}$$

where R and L denote the load resistance and inductance, respectively. In addition, $\boldsymbol{v}_{abc}$ and $\boldsymbol{i}_{abc}$ represent the voltage vector generated by the VSI and the load current vector in the *abc* frame, respectively. The derivative of the load current in the continuous-time model can be approximated on the basis of the forward Euler approximation with sampling period $T_{\rm sp}$ as

$$\frac{d\boldsymbol{i}_{abc}}{dt} \approx \frac{\boldsymbol{i}_{abc}\,(k+1) - \boldsymbol{i}_{abc}\,(k)}{T_{\rm sp}}. \tag{2}$$

The load current dynamic of (1) can then be represented in the discrete-time domain as

$$\boldsymbol{i}_{abc}\,(k+1) = \left(1 - \frac{RT_{\rm sp}}{L}\right)\boldsymbol{i}_{abc}\,(k) + \frac{T_{\rm sp}}{L}\boldsymbol{v}_{abc}\,(k). \tag{3}$$

Assuming that the one-step future load currents become equal to the one-step future current references by applying the voltage reference, the load dynamic in (3) can be expressed by the inverse dynamic model as [16], [17]

$$\boldsymbol{v}^*_{abc}\,(k) = \frac{1}{T_{\rm sp}}\left\{L\boldsymbol{i}^*_{abc}\,(k+1) + (RT_{\rm sp} - L)\,\boldsymbol{i}_{abc}\,(k)\right\}. \tag{4}$$

B. Delay Compensation

By shifting the inverse model in (4) by one-step forward, the future voltage reference at the $(k+1)$th instant is obtained as

$$\begin{aligned}\boldsymbol{v}^*_{abc}\,(k+1) = \frac{1}{T_{\rm sp}}\big\{&L\boldsymbol{i}^*_{abc}\,(k+2)\\ &+ (RT_{\rm sp} - L)\,\boldsymbol{i}_{abc}\,(k+1)\big\}.\end{aligned} \tag{5}$$

At the kth instant, the one-step future load current $\boldsymbol{i}_{abc}(k+1)$ required in (5) can be calculated by measuring the present load current $\boldsymbol{i}_{abc}(k)$ and the present VSI voltage application $\boldsymbol{v}_{abc}(k)$, as shown in (3). Furthermore, the one-step future current reference $\boldsymbol{i}^*_{abc}(k+1)$ can be calculated from the Lagrange extrapolation using the present and the two past reference values as [4]

$$\boldsymbol{i}^*_{abc}\,(k+1) = 3\boldsymbol{i}^*_{abc}\,(k) - 3\boldsymbol{i}^*_{abc}\,(k-1) + \boldsymbol{i}^*_{abc}\,(k-2). \tag{6}$$

The two-step future current reference $\boldsymbol{i}^*_{abc}(k+2)$ required in (5) can be obtained by shifting by one-step forward the future current reference $\boldsymbol{i}^*_{abc}(k+1)$ in (6) as

$$\boldsymbol{i}^*_{abc}\,(k+2) = 3\boldsymbol{i}^*_{abc}\,(k+1) - 3\boldsymbol{i}^*_{abc}\,(k) + \boldsymbol{i}^*_{abc}\,(k-1). \tag{7}$$

Considering the inevitable delay existing inside the controller, the control steps are modified on the basis of (5) to compensate for the control delay as follows:

1) measuring the load current $\boldsymbol{i}_{abc}(k)$ at the kth instant;
2) applying the kth VSI voltage $\boldsymbol{v}_{abc}(k)$, which was determined by $\boldsymbol{v}^*_{abc}(k)$ calculated in the previous interval;
3) predicting the $(k+1)$th load current $\boldsymbol{i}_{abc}(k+1)$ with $\boldsymbol{i}_{abc}(k)$ and $\boldsymbol{v}_{abc}(k)$ using (3);
4) calculating the $(k+2)$th load current reference $\boldsymbol{i}^*_{abc}(k+2)$ using (6) and (7);
5) predicting the future voltage reference $\boldsymbol{v}*_{abc}(k+1)$ in (5), which is stored for application at the beginning of the next $(k+1)$th sampling instant.

By applying the delay compensation technique, almost one sampling period can be assigned for the calculations and predictions required to determine the optimal voltage vector. Because the VSI can only generate seven possible voltage states, the seven voltage states are evaluated by a predefined cost function to select one optimal state closest to the future voltage reference in (5). By applying the optimal voltage state to the load, the load current generated by the VSI at the next sampling instant can track the future current reference.

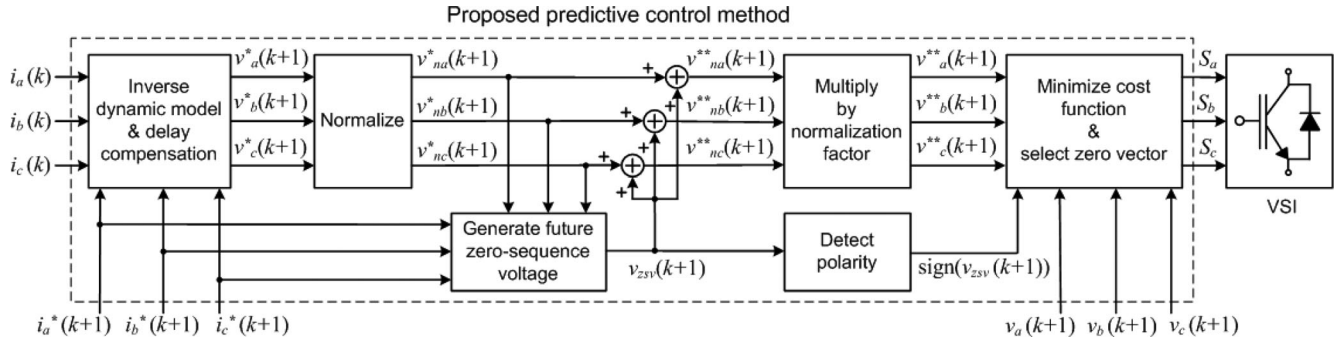

Fig. 3. Block diagram of the proposed predictive control method with zero-sequence voltage injection to reduce switching loss.

C. Predictive Control Method With Future Voltage References Modified by Zero-Sequence Voltage Injection

In this study, the three-phase future voltage reference in (5) is modified by injecting the future zero-sequence voltage to minimize the VSI switching loss. Fig. 3 shows the overall block diagram of the proposed predictive control method with the zero-sequence voltage injection. The three-phase future voltage references achieved by the inverse dynamic model in (5), i.e., $v_a^*(k+1)$, $v_b^*(k+1)$, and $v_c^*(k+1)$, are normalized by dividing them with the peak value to limit their magnitude within ± 1. The peak value for the normalization is obtained by

$$V_{pk}^*(k+1) = \sqrt{(v_\alpha^*(k+1))^2 + (v_\beta^*(k+1))^2} \tag{8}$$

where $v_\alpha^*(k+1)$ and $v_\beta^*(k+1)$ are the α and β components of the *abc* voltage vector $v_{abc}\ (k+1)$ achieved by the *abc*-to-$\alpha\beta$ transformation given by

$$v_\alpha^*(k+1) = (1/3)\left\{2v_a^*(k+1) - v_b^*(k+1) - v_c^*(k+1)\right\}$$
$$v_\beta^*(k+1) = \left(1\Big/\sqrt{3}\right)\left\{v_b^*(k+1) - v_c^*(k+1)\right\}.$$

The instantaneous switching losses depend on the magnitude of the load current flowing through the leg of the VSI at the instant of switching [16]. Thus, the future zero-sequence voltage in the proposed method is generated in such a manner that the three-phase future voltage references modified by the future zero-sequence voltage injection can clamp one leg that conducts the largest load current to either the positive or negative dc-link. Fig. 4 shows the flowchart of the generation of the future zero-sequence voltage to reduce the switching loss in the proposed predictive control method. The three normalized future voltage references obtained by the inverse dynamic model are sorted on the basis of their magnitudes and are assigned as

$$v_{\max}^*(k+1) = \text{MAX}\left[v_{na}^*(k+1), v_{nb}^*(k+1), v_{nc}^*(k+1)\right]$$
$$v_{\text{mid}}^*(k+1) = \text{MID}\left[v_{na}^*(k+1), v_{nb}^*(k+1), v_{nc}^*(k+1)\right]$$
$$v_{\min}^*(k+1) = \text{MIN}\left[v_{na}^*(k+1), v_{nb}^*(k+1), v_{nc}^*(k+1)\right]. \tag{9}$$

The normalized future voltage references are used to detect a prohibitive phase that should not be clamped to avoid overmodulation of at least another phase because clamping a nonallowed-phase leads to overmodulation of at least another phase; consequently, the overmodulation results in loss of the current controllability of the VSI [15]. The prohibitive phase, which should be prevented from being clamped, corresponds to the phase with medium voltage $v_{\text{mid}}^*(k+1)$ to ensure that the VSI operates within the linear modulation range. Therefore, $v_{\text{mid}}^*(k+1)$ is excluded in the process to generate the zero-sequence voltage. As a result, one of the two remaining legs associated with $v_{\max}^*(k+1)$ and $v_{\min}^*(k+1)$ must be clamped to either the positive or negative dc-link, depending on which leg conducts a larger load current. For example, when the leg assigned to $v_{\max}^*(k+1)$, which should be positive, conducts a current with a higher magnitude, the future zero-sequence voltage is generated so as to clamp the upper switch in the leg with $v_{\max}^*(k+1)$ to the positive dc-link. Thus, the modified voltage references with the future zero-sequence voltage injection prevent one leg with the largest load current from switching. Because the future zero-sequence voltage is optimized online on the basis of the future voltage and current references, as shown in Fig. 4, the proposed algorithm to determine the clamping leg does not require extra calculation about the load power factor. Moreover, because the future zero-sequence voltage is calculated on the basis of the sampling period, the clamping region is adaptively shifted depending on the load angle. Therefore, the proposed predictive control method can reduce the switching losses at any operating point, including transient and steady-state conditions.

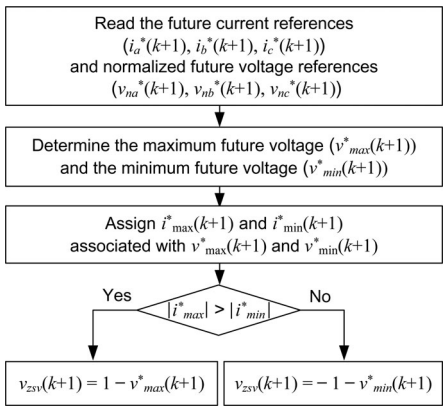

Fig. 4. Flowchart of the future zero-sequence voltage generation in the proposed predictive control method.

TABLE I
VALID EIGHT SWITCHING STATES AND CORRESPONDING LOAD PHASE VOLTAGES OF THE VSI

Voltage state	S_a	S_b	S_c	v_a	v_b	v_c
V_0	0	0	0	0	0	0
V_1	0	0	1	$-V_{dc}/3$	$-V_{dc}/3$	$2V_{dc}/3$
V_2	0	1	0	$-V_{dc}/3$	$2V_{dc}/3$	$-V_{dc}/3$
V_3	0	1	1	$-2V_{dc}/3$	$V_{dc}/3$	$V_{dc}/3$
V_4	1	0	0	$2V_{dc}/3$	$-V_{dc}/3$	$-V_{dc}/3$
V_5	1	0	1	$V_{dc}/3$	$-2V_{dc}/3$	$V_{dc}/3$
V_6	1	1	0	$V_{dc}/3$	$V_{dc}/3$	$-2V_{dc}/3$
V_7	1	1	1	0	0	0

The modified future voltage reference with the future zero-sequence voltage injection is, as shown in Fig. 3, assessed by a cost function defined as

$$g = |v_a^{**}(k+1) - v_a(k+1)| + |v_b^{**}(k+1) - v_b(k+1)| + |v_c^{**}(k+1) - v_c(k+1)| \quad (10)$$

where $v_i \in \{0, \pm V_{\rm dc}/3, \pm 2V_{\rm dc}/3\}$, $i = a, b$, and c. The valid eight switching states and the corresponding VSI voltage states are listed in Table I. The proposed predictive control scheme that uses the cost function selects the optimal switching state, which can generate the optimal output voltage state closest to the modified future voltage reference. The cost function predetermined to minimize the errors between the voltage references and the VSI output voltages selects the optimal switching state in the next step. Because the future voltage reference is modified to ensure clamping of one leg with the largest current, the proposed predictive control method can reduce the switching loss and perform current control to track the current references.

Although the two zero vectors result in the same output voltage to the load, improper selection of the zero vector might lead to unnecessary switching operation, which increases the switching loss. Because selecting the switching state using only the cost function cannot provide the optimal choice of the zero vector in terms of the switching loss, this study develops an optimal zero-vector selection using the future zero-sequence voltage to reduce the switching losses. In the case where the zero vector is selected as the optimal voltage state by the cost function, the polarity of the future zero-sequence voltage decides which zero vector is utilized, as shown in Fig. 5. When voltage v_{zsv} is positive and negative, zero vectors V_7 and V_0 are employed, respectively. This selection of the zero vectors enables the switching patterns to maintain the clamping period with no switching operation, as shown in Fig. 5.

The block diagrams in Figs. 2 and 3 clearly show that the proposed predictive control method can be implemented with no additional measurement because the future current and voltage references required to construct the future zero-sequence voltage are already available inside. Note that, although the actual future output currents may also be utilized to generate the future zero-sequence voltage, it might result in the delay of one sampling period as well as in waveform distortion because of the current ripples. Therefore, the future current references are used to produce the zero-sequence voltage in the proposed control method. In the proposed predictive control method, only two phases are modulated, and one phase with the largest load current, if it is not the prohibitive phase, is clamped to the positive or negative dc-bus bar. The modified future voltage references with the zero sequence voltage and the optimal distribution of the zero vector by the proposed method can lead to high efficiency with the reduced switching losses of the VSI.

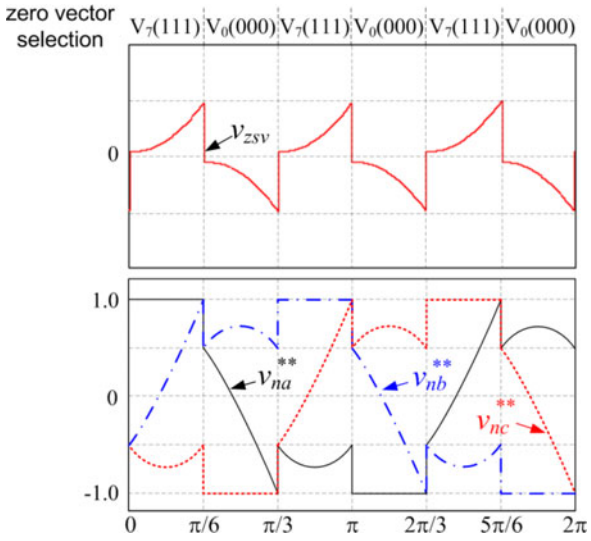

Fig. 5. Selection method of the zero vector.

III. SIMULATION RESULTS

Fig. 6 shows the simulated waveforms obtained by the proposed predictive control method at different load angles, where the filtered voltage references v_{na}^{*} and v_{na}^{**} are shown for clarity. The proposed predictive control method prevents switch S_a of the VSI from switching in the vicinity of the largest ranges of the load current i_a. In addition, the clamping period generated by the proposed predictive control method moves and splits, depending on the load angles. Fig. 6(a) shows that the proposed predictive control features DPWM 1, where the center of the clamped region is aligned with the peak of the current and voltage references, with loads of almost unity power factor. Furthermore, the proposed predictive control method can produce the same switching pattern with DPWMs 2 and 3 at 30° and 90° load angles, respectively, as shown in Fig. 6(b) and (d). Therefore, the proposed predictive control method can result in the switching patterns to reduce the switching losses irrespective of the load angle.

For purpose of comparison, Fig. 7 shows the normalized a-phase reference current i_a and the switching signal S_a obtained from the conventional predictive control method with different load angles. Because the conventional predictive control method is, in general, realized with only one zero state between V_0 and V_7, the waveforms using the zero state V_0 are illustrated in Fig. 7. As seen from Fig. 7, the conventional predictive control method produces the switching pulse patterns with spontaneous

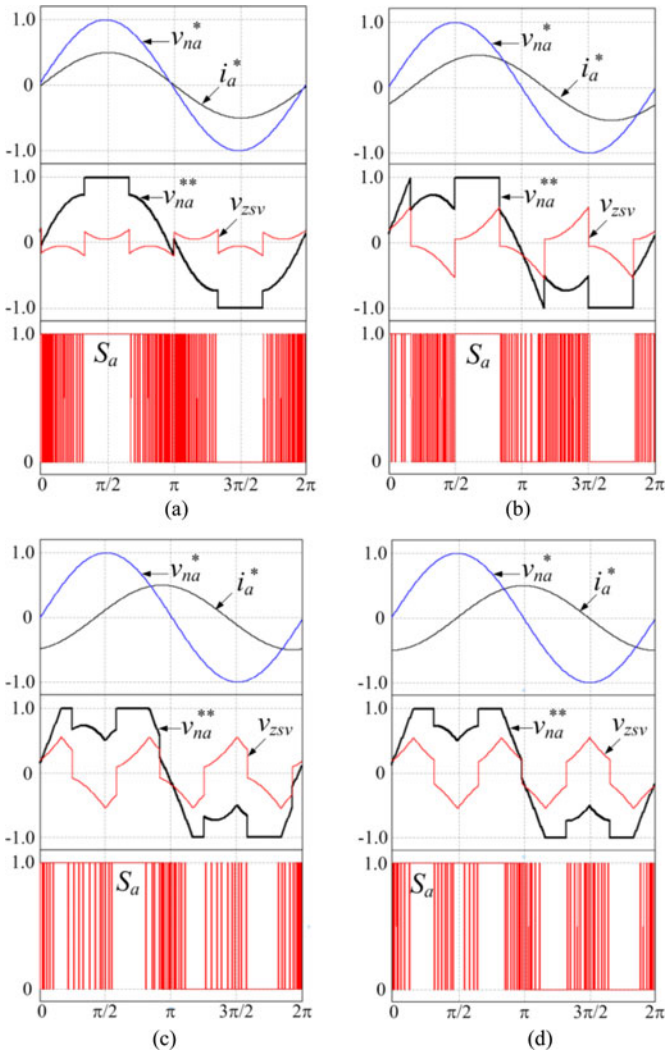

Fig. 6. Simulated waveforms of current reference i_a^*, filtered reference voltage v_{na}^*, future zero-sequence voltage v_{zsv}, filtered future reference voltage with zero-sequence voltage injection v_{na}^{**}, and a-phase upper switching signal S_a of the proposed method ($T_{\rm sp} = 50$ μs, $I^* = 0.5$ A, and $V_{\rm dc} = 200$ V) with (a) $\phi \approx 0°$, (b) $\phi = 30°$, (c) $\phi = 75°$, and (d) $\phi \approx 90°$.

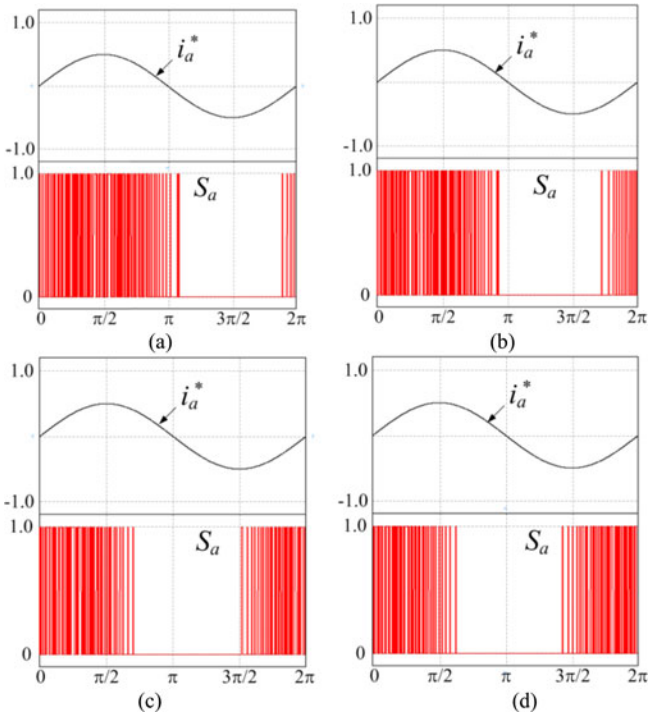

Fig. 7. Simulated waveforms of current reference i_a^* and a-phase upper switching signal S_a of the conventional predictive control method ($T_{\rm sp} = 50$ μs, $I^* = 0.5$ A, and $V_{\rm dc} = 200$ V) with (a) $\phi \approx 0°$, (b) $\phi = 30°$, (c) $\phi = 75°$, and (d) $\phi \approx 90°$.

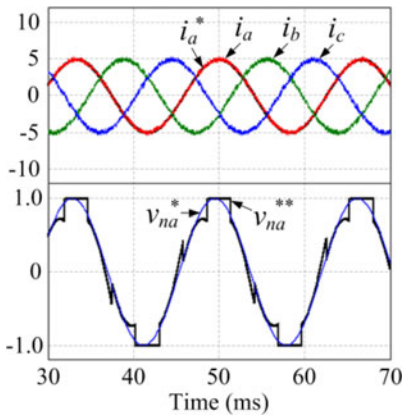

Fig. 8. Simulated waveforms of the three-phase load currents, current reference i_a^*, filtered reference voltage v_{na}^*, and filtered future reference voltage with zero-sequence voltage injection v_{na}^{**} of the proposed method ($T_{\rm sp} = 50$ μs, $I^* = 5$ A, $\phi = 10°$, and $V_{\rm dc} = 100$ V).

clamping periods, where the a-phase clamps to the negative dc-link with no successive switching operations. It should be noted that the a-phase ties to the positive dc-link during the same clamping interval, in the case where the conventional method employs the zero state V_7. In addition, the spontaneous clamping periods generated by the conventional method slides right to left as the load angle increases.

Fig. 8 shows the simulation results of the three-phase load currents along with the a-phase current reference achieved from the proposed predictive control method with the zero-sequence voltage. The load current obtained by the proposed control method accurately tracks the current reference with one leg exposed to the largest load current clamped to the dc-link by the future voltage reference.

Performances of the predictive control methods due to its inherent operating principle are strongly influenced by the sampling period. Thus, the proposed predictive control method with the zero-sequence voltage injection as a function of the sampling period is compared with the conventional predictive control method shown in Fig. 2 in terms of the average switching frequency, loss, current errors, and total harmonic distortions (THDs) of the load currents, as shown in Fig. 9. For fair comparison, the proposed method is compared with the conventional method with the delay compensation [12].

The average switching frequency is defined as

$$f_{\rm sw,avg} = \sum_{i=a,b,c} \frac{f_{{\rm sw},i}}{3}. \tag{11}$$

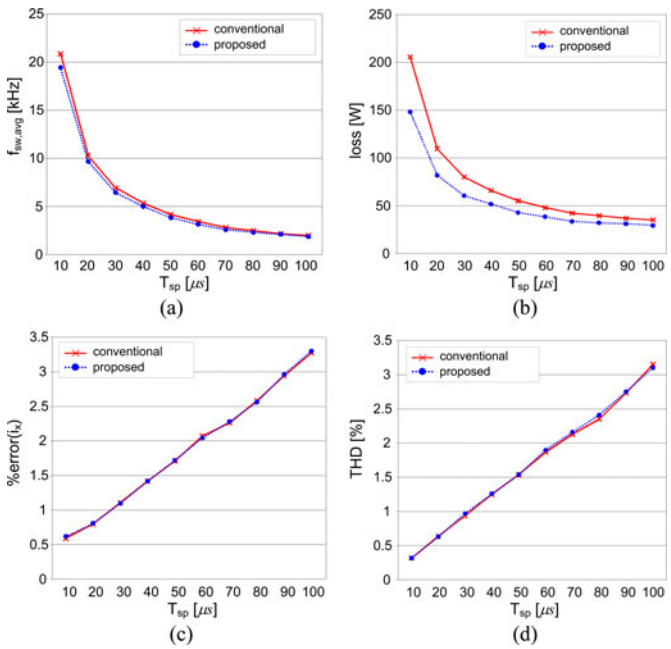

Fig. 9. Comparison results of the proposed and the conventional predictive control methods as a function of the sampling periods in terms of (a) average switching frequency, (b) semiconductor loss, (c) current error, and (d) THD ($V_{\rm dc} = 200$ V, $I^* = 9$ A, $R = 1.5\ \Omega$, and $L = 14$ mH).

The switching frequency of each leg is calculated by measuring the number of switching operations of the switches for 15 output periods. Because both the conventional and the proposed methods have the clamping periods as shown in Figs. 6 and 7, the proposed method with the zero-sequence voltage shows slightly lower average switching frequency than the conventional method, as shown in Fig. 9(a). The semiconductor losses obtained from the two methods are shown in Fig. 9(b). The VSI semiconductor losses, including the conduction and switching losses, are simulated on the basis of the VSI loss model [18], [19]. The conduction losses of an IGBT or a diode in the VSI are calculated on the basis of the first-order curve fitting using the on-state voltage drop and the conduction current obtained from the simulation model [18]. The data were chosen from the EUPEC IGBT module SK60GM123 with 1200-V and 60-A ratings. The switching losses were similarly determined by measuring the switching energy as a function of the conducting current through the switch and then modeling the energy using a first-order relationship. The turn-on and turn-off switching energies were also determined from the data sheet according to the conduction currents. A constant junction temperature $T_j = 125\ ^\circ$C was used for the loss performance calculation. The loss of the proposed method is lower than that of the conventional method because of the decreased switching loss due to the clamping operation resulting from the future zero-sequence voltage. Fig. 9(c) shows the percentages of the current errors obtained by the conventional and proposed predictive control methods versus the sampling period. The percentage of the current error is defined as the absolute difference between the reference and the load currents normalized to the respective rms value of the load current references as

$$\%\text{error}(i_x) = \frac{\sum_{x=a,b,c} \frac{1}{N} \sum_{k=1}^{N} |i_x^*(k) - i_x(k)|}{\sum_{x=a,b,c} \text{rms}(i_x^*(k))} \times 100 \tag{12}$$

where N is 20 000 per fundamental output period. The two control methods have almost same current-tracking capability, as shown in Fig. 9(c). Fig. 9(d) shows the THD percentages obtained by the predictive control method as a function of the sampling period. The THD percentage is defined as

$$\%\text{THD} = \frac{\sum_{x=a,b,c} \sqrt{i_{x2}^2 + i_{x3}^2 + \cdots + i_{xn}^2}}{\sum_{x=a,b,c} i_{x1}} \times 100 \tag{13}$$

where i_{x1} and i_{xn} are the fundamental and nth-harmonic components of the load current in phase x, respectively. The number n was set to 8335 in the simulation. Fig. 9(d) shows that the proposed predictive control method exhibits a slightly higher THD than the conventional method because of the clamping operation.

IV. Experimental Results

The proposed predictive control method with the future zero-sequence voltage for switching loss reduction was tested using a prototype setup. The setup consisted of a three-phase VSI with an IGBT module and an *RL* load. The entire switching algorithm with current control was implemented in a DSP board (TMS320F28335) with sampling period $T_{\rm sp} = 50\ \mu$s to generate sinusoidal load currents with a 60-Hz fundamental output frequency.

Fig. 10 shows the experimental waveforms of the filtered a-phase voltage reference v_{na}^*, the a-phase current reference i_a^*, the future zero-sequence voltage v_{zsv}, and the filtered a-phase modified voltage reference v_{na}^{**} obtained from the proposed predictive control method at different load angles. Fig. 10 shows that the shape of the modified voltage reference v_a^{**} in the proposed method is similar to that in the simulation results shown in Fig. 6. The proposed method clearly shapes the modified voltage reference v_a^{**} with a clamping period to prevent switching operation in the vicinity of the largest load currents. In addition, the clamping period obtained by v_a^{**} automatically varied with the load angles to reduce the switching losses.

The a-phase load current and load voltage without and with the delay compensation, obtained by the proposed predictive control method, are shown in Fig. 11. The ripples in the load current are clearly reduced, and the effective switching frequency increases when the compensation algorithm of the control delay is applied.

Figs. 12 and 13 show the experimental results of the three-phase load currents, along with the a-phase current reference and the a-phase normalized future voltage references, achieved from the proposed predictive control method with the zero-sequence voltage. The load currents controlled by the proposed method accurately track the current reference, whereas the future voltage reference v_{na}^{**} with the zero-sequence voltage stops the switching operation during the clamping period.

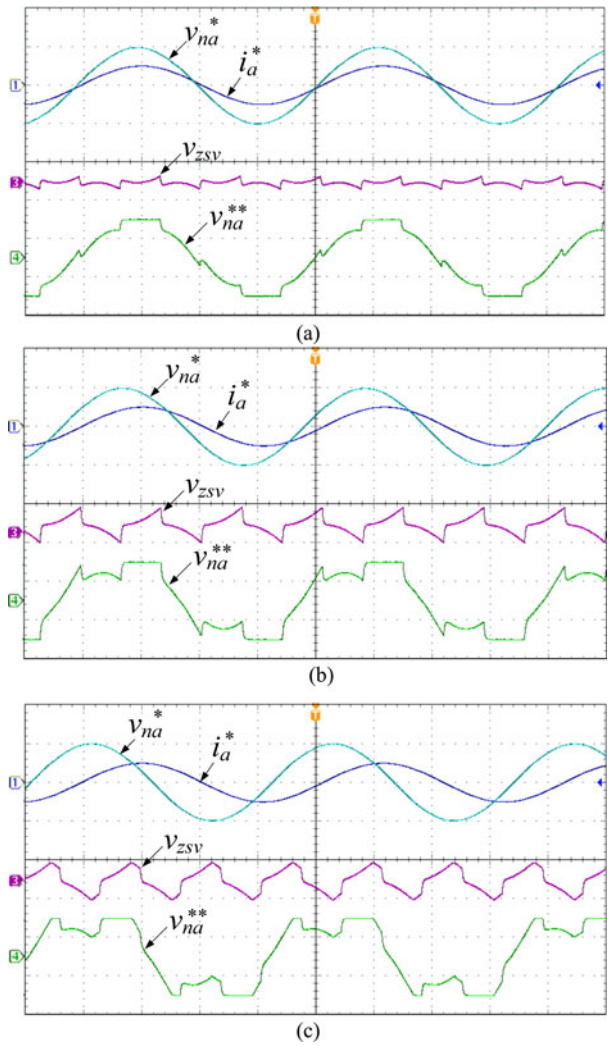

Fig. 10. Experimental waveforms of the filtered a-phase voltage reference v_{na}^*, a-phase current reference i_a^*, zero-sequence voltage v_{zsv}, and filtered a-phase modified voltage reference v_{na}^{**} of the proposed predictive control method at different load angles (a) $\phi = 6.0°$ (b) $\phi = 29.5°$, and (c) $\phi = 74.0°$ ($T_s = 50$ μs, $I^* = 1$ A, and $V_{\rm dc} = 100$ V).

The dynamic responses of the proposed and conventional predictive control method for sampling time $T_{\rm sp} = 50$ μs are shown in Figs. 14 and 15 at a 10° load angle. The reference current has a step change in the frequency command from 60 to 90 Hz, as shown in Fig. 14, whereas the magnitude of the reference currents is subjected to a half-step change, as shown in Fig. 15. It can be observed that the three-phase load currents controlled by the proposed method follow the reference change with fast dynamics under both step changes. In addition, the switching signal of switch S_a is displayed in the transient responses. Clearly, the switching operations of S_a obtained from the proposed method in Figs. 14(a) and 15(a) are stopped in the vicinity of the peak of current i_a regardless of the transient responses. On the other hand, the switching operation S_a of the conventional control method using the zero vector V_0 stops in only the areas of the negative load current i_a in Figs. 14(b) and 15(b).

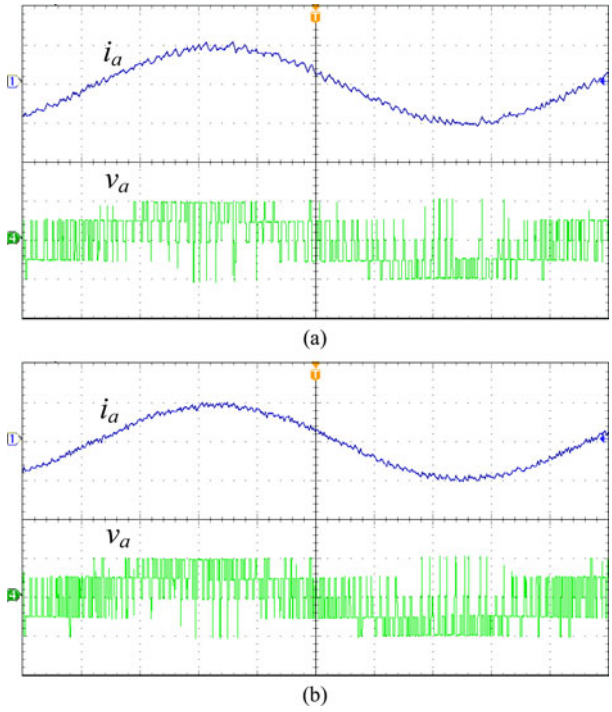

Fig. 11. Experimental waveforms of the a-phase load current (i_a) (2 A/div and 2 ms/div) and the a-phase load voltage (v_a) (70 V/div and 2 ms/div) from (a) without delay compensation and (b) with delay compensation ($I^* = 2$ A, $T_{\rm sp} = 50$ μs, $V_{\rm dc} = 100$ V, $R = 20$ Ω, and $L = 10$ mH).

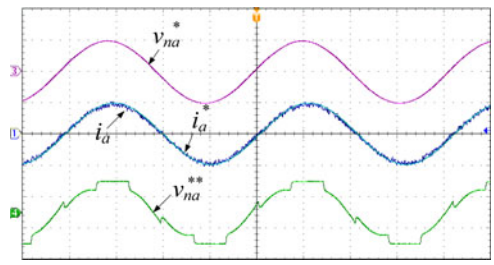

Fig. 12. Experimental waveforms of the filtered a-phase voltage reference v_{na}^*, a-phase load current (i_a), a-phase current reference (i_a^*) (2 A/div and 2 ms/div), and filtered a-phase modified voltage reference v_{na}^{**} of the proposed predictive control method ($I^* = 2$ A, $T_{\rm sp} = 50$ μs, $V_{\rm dc} = 100$ V, $R = 20$ Ω, and $L = 10$ mH).

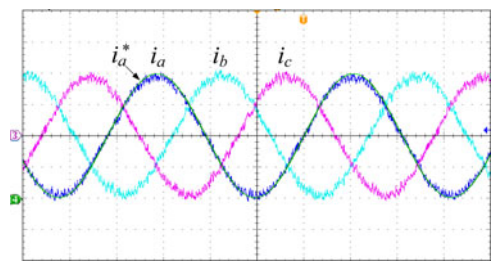

Fig. 13. Experimental waveforms of the three-phase load currents (i_a, i_b, and i_c) and a-phase reference current (i_a^*) (1 A/div and 4 ms/div) obtained from the proposed predictive control method ($I^* = 2$ A, $T_{\rm sp} = 50$ μs, $V_{\rm dc} = 100$ V, $R = 20$ Ω, and $L = 10$ mH).

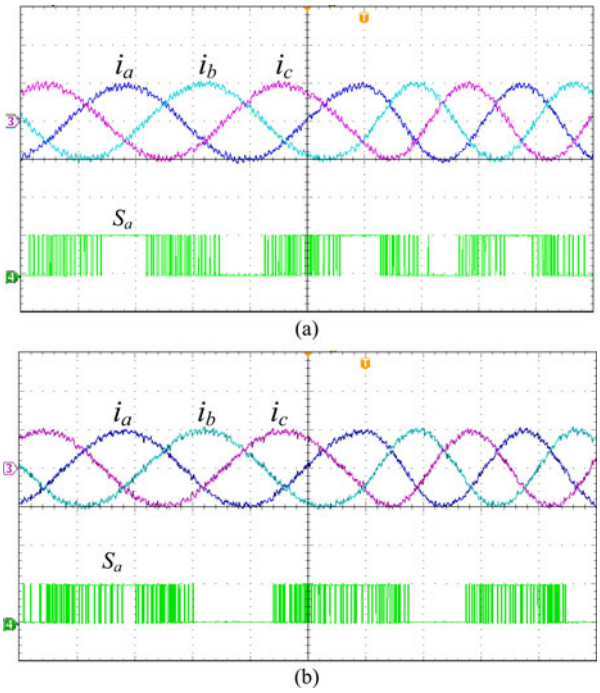

Fig. 14. Experimental waveforms of the three-phase load currents (i_a, i_b, and i_c) and a-phase upper switching signal S_a under a frequency-step change from 60 to 90 Hz (2 A/div and 4 ms/div) of (a) the proposed method (b) the conventional model predictive method ($I^* = 2$ A, $T_{\rm sp} = 50$ μs, $V_{\rm dc} = 100$ V, $R = 20$ Ω, and $L = 10$ mH).

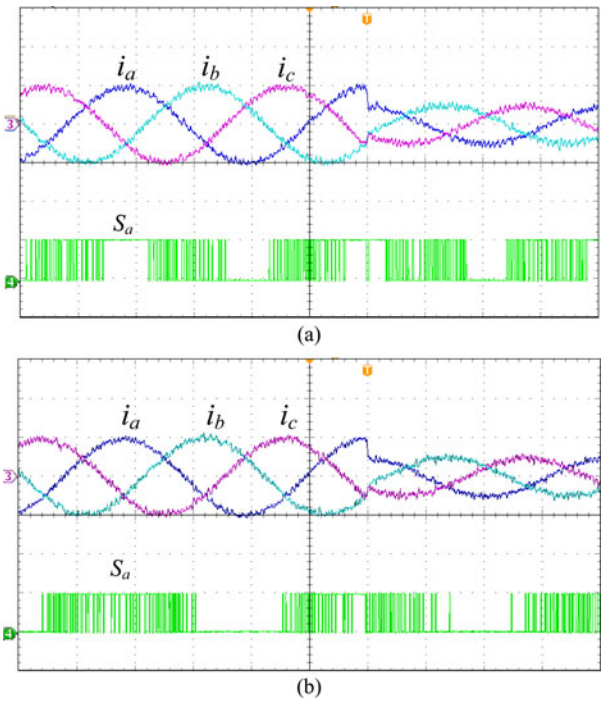

Fig. 15. Experimental waveforms of the three-phase load currents (i_a, i_b, and i_c) and a-phase upper switching signal S_a under a magnitude-step change (2 A/div and 4 ms/div) of (a) the proposed method (b) the conventional model predictive method ($I^* = 2$ A, $T_{\rm sp} = 50$ μs, $V_{\rm dc} = 100$ V, $R = 20$ Ω, and $L = 10$ mH).

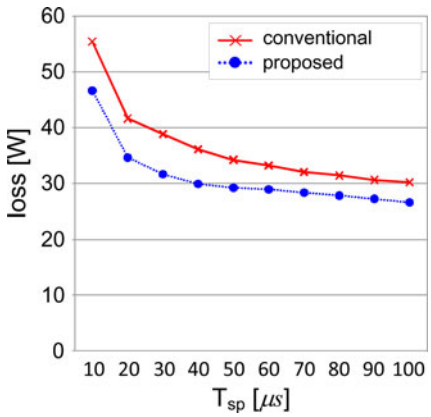

Fig. 16. Experimental results of the total losses from the conventional and proposed methods versus the load angles under constant power ($V_{\rm dc} = 200$ V, $I^* = 9$ A, $R = 1.5$ Ω, and $L = 14$ mH).

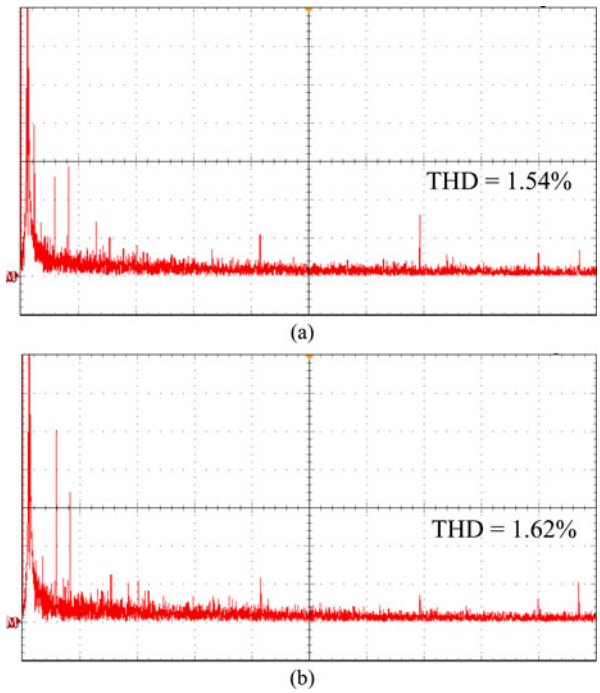

Fig. 17. Frequency spectrum of the load current (i_a) (500 Hz/div and 5 mA/div) obtained from the (a) conventional and (b) proposed predictive control methods ($I^* = 9$ A, $T_{\rm sp} = 50$ μs, $V_{\rm dc} = 200$ V, $R = 1.5$ Ω, and $L = 14$ mH).

The experimental loss data obtained from the conventional and the proposed predictive control methods under several sampling periods are shown in Fig. 16. The input and output power data of the VSI are measured using the power analysis application module (DPO3PWR) in the Tektronix digital oscilloscope (500 MHz MSO3054) to calculate the losses in the experimental setup. Both predictive control methods are tested using the delay compensation algorithm for fair comparison. It can be seen that the proposed method with the zero-sequence voltage generates a semiconductor loss lesser than that of the conventional method for all the considered sampling periods, as shown in Fig. 16. The frequency spectra of the load currents obtained from the conventional and proposed methods are shown in Fig. 17, where the proposed method results in slightly higher THD.

V. Conclusion

This paper has proposed a predictive control method with the injection of future zero-sequence voltage to efficiently reduce the switching losses of three-phase VSIs. The three-phase future voltage references modified by the future zero-sequence voltage injection in the proposed predictive control method are generated so as to clamp one of the three legs with the largest load current. In addition, future voltage references are realized with the delay compensation for the inevitable control delay, leading to reduced load current ripples. The future zero-sequence voltage, which is produced online with the future voltage and current references on the basis of the sampling period, optimally adjusts the clamping duration on each leg, depending on the load angle. In addition, the proposed method develops the zero-vector selection using the future zero-sequence voltage to minimize the switching losses. Therefore, the proposed predictive control method can perform load current control and minimize the switching losses of the VSIs under any load condition. The simulation and experimental results verify the effectiveness of the proposed predictive control method.

References

[1] M. P. Kazmierkowski, R. Krishnan, and F. Blaabjerg, *Control in Power Electronics*. New York, NY, USA: Academic, 2002.

[2] Y. He, J. Liu, Z. Wang, and Y. Zou, "A PI control algorithm with zero static misadjustment for tracking the harmonic current of three-level APFs," *J. Power Electron.*, vol. 14, no. 1, pp. 175–182, Jan. 2014.

[3] S. Kouro, P. Cortes, R. Vargas, U. Ammann, and J. Rodriguez, "Model predictive control—A simple and powerful method to control power converters," *IEEE Trans. Ind. Electron.*, vol. 56, no. 6, pp. 1826–1838, Jun. 2009.

[4] J. Rodrguez, J. Pontt, C. Silva, P. Correa, P. Lezana, P. Cortés, and U. Ammann, "Predictive current control of a voltage source inverter," *IEEE Trans. Ind. Electron.*, vol. 54, no. 1, pp. 495–503, Feb. 2007.

[5] R. Vargas, P. Cortes, U. Ammann, J. Rodriguez, and J. Pontt, "Predictive control of a three-phase neutral-point-clamped inverter," *IEEE Trans. Ind. Electron.*, vol. 54, no. 5, pp. 2697–2705, Oct. 2007.

[6] P. Cortes, J. Rodriguez, P. Antoniewicz, and M. Kazmierkowski, "Direct power control of an AFE using predictive control," *IEEE Trans. Power Electron.*, vol. 23, no. 5, pp. 2516–2523, Sep. 2008.

[7] V. Yaramasu, M. Rivera, B. Wu, and J. Rodriguez, "Model predictive current control of two-level four-leg inverters—part I: Concept, algorithm, and simulation analysis," *IEEE Trans. Power Electron.*, vol. 28, no. 7, pp. 3459–3468, Jul. 2013.

[8] M. Preindl and S. Bolognani, "Model predictive direct speed control with finite control set of PMSM drive systems," *IEEE Trans. Power Electron.*, vol. 28, no. 2, pp. 1007–1015, Feb. 2013.

[9] C. D. Townsend, T. J. Summers, J. Vodden, A. J. Watson, R. E. Betz, and J. C. Clare, "Optimization of switching losses and capacitor voltage ripple using model predictive control of a cascaded H-bridge multilevel statcom," *IEEE Trans. Power Electron.*, vol. 28, no. 7, pp. 3077–3087, Jul. 2013.

[10] R. Vargas, U. Ammann, B. Hudoffsky, J. Rodriguez, and P. Wheeler, "Predictive torque control of an induction machine fed by a matrix converter with reactive input power control," *IEEE Trans. Power Electron.*, vol. 25, no. 6, pp. 1426–1438, Jun. 2010.

[11] Y. Atis and M. Salem, "Microcontroller-based improved predictive current controlled VSI for single-phase grid-connected systems," *J. Power Electron.*, vol. 13, no. 6, pp. 1016–1023, Nov. 2013.

[12] P. Cortes, J. Rodriguez, C. Silva, and A. Flores, "Delay compensation in model predictive current control of a three-phase inverter," *IEEE Trans. Ind. Electron.*, vol. 59, no. 2, pp. 1323–1325, Feb. 2012.

[13] J. Rodriguez, M. P. Kazmierkowski, J. R. Espinoza, P. Zanchetta, H. Abu-Rub, H. A. Young, and C. A. Rojas, "State of the art of finite control set model predictive control in power electronics," *IEEE Trans. Ind. Informat.*, vol. 9, no. 2, pp. 1003–1016, May 2013.

[14] A. M. Hava, R. J. Kerkman, and T. A. Lipo, "A high-performance generalized discontinuous PWM algorithm," *IEEE Trans. Ind. Appl.*, vol. 34, no. 5, pp. 1059–1071, Sep./Oct. 1998.

[15] L. Asiminoaei, P. Rodriguez, F. Blaabjerg, and M. Malinowski, "Reduction of switching losses in active power filters with a new generalized discontinuous-PWM strategy," *IEEE Trans. Ind. Electron.*, vol. 55, no. 1, pp. 467–471, Jan. 2008.

[16] J. Barros, J. Silva, and E. Jesus, "Fast-predictive optimal control of NPC multilevel converters," *IEEE Trans. Ind. Electon.*, vol. 60, no. 2, pp. 619–627, Feb. 2013.

[17] M. Perez, P. Cortes, and J. Rodriguez, "Predictive control algorithm technique for multilevel asymmetric cascaded H-bridge inverters," *IEEE Trans. Ind. Electon.*, vol. 55, no. 12, pp. 4354–4361, Dec. 2008.

[18] F. Blaabjerg, U. Jaeger, S. M. Nielsen, and J. K. Pedersen, "Power losses in PWM-VSI inverter using NPT or PT IGBT devices," *IEEE Trans. Power Electon.*, vol. 10, no. 3, pp. 358–367, May 1995.

[19] S. Bernet, S. Ponnaluri, and R. Teichmann, "Design and loss comparison of matrix converters and voltage-source converters for modern AC drives," *IEEE Trans. Ind. Electron.*, vol. 49, no. 2, pp. 304–314, Apr. 2002.

Sangshin Kwak (S'02–M'05) received the Ph.D. degree in electrical engineering from Texas A&M University, College Station, TX, USA, in 2005.

From 1999 to 2000, he worked as a Research Engineer at LG Electronics, Changwon, Korea. He was also with Whirlpool R&D Center, Benton Harbor, MI, USA, in 2004. From 2005 to 2007, he worked as a Senior Engineer in Samsung SDI R&D Center, Yongin, Korea. From 2007 to 2010, he worked as an Assistant Professor at Daegu University, Gyeongsan, Korea. Since 2010, he has been with Chung-Ang University, Seoul, Korea, currently as an Associate Professor. His research interests include topology design, modeling, control, and analysis of ac/dc, dc/ac, and ac/ac power converters including resonant converters for adjustable speed drives and digital display drivers as well as modern control theory applied to DSP-based power electronics.

Jun-Cheol Park received the B.S. degree in electrical and electronics engineering from Chung-Ang University, Seoul, Korea, in 2013, where he is working toward the M.S. degree in electrical and electronics engineering.

His research interests include predictive control and analysis for multilevel inverters, voltage source inverters, active front ends, and active power filters.